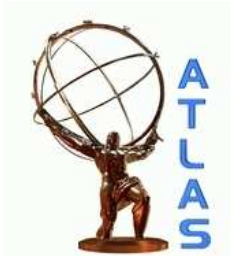

ATLAS NOTE

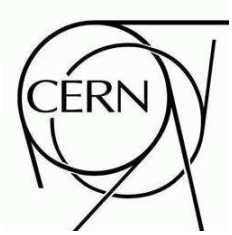

The Effect of Tile Light Collection Reduction along Radius on the ATLAS Tile Calorimeter Uniformity

S.Errede[1)], A.Henriques[2)], A.Isaev[3)] , A.Karyukhin[3)],
H.Khandanyan[1)], M.Makouski[3)], A.Myagkov[3)], N.Shalanda[3)],
A.Solodkov[3)], O.Solovyanov[3)], E.Starchenko[3)], I.Vichou[1)]

ATL-TILECAL-PUB-2009-005
13 March 2009

Abstract

We report on the light collection non-uniformity of trapezoidal scintillating tiles along the ATLAS detector radius and its consequence on the miscalibration of the middle and rear longitudinal calorimeter samplings. We discuss the need to apply additional corrections to the cell response after equalization and corrections obtained from the cesium calibration system in order to bring all three longitudinal samplings to the proper electromagnetic scale.

[1)] University of Illinois, Urbana–Champaign, Illinois, USA
[2)] CERN, Geneva, Switzerland
[3)] Institute for High Energy Physics, Protvino, Russia

Contents

1 Introduction to Tilecal

The ATLAS detector is a general-purpose experiment designed to exploit the full extent of the exciting physics opportunities for fundamental discoveries at LHC [1]. One of the major components of ATLAS calorimetry is the Tile Hadronic Calorimeter (TileCal) [2]. TileCal is composed of a Long Barrel (LB) and two Extended Barrel (EB) cylindrical structures spanning the pseudorapidity region $|\eta| \leq 1.7$. Azimuthally, the barrel and extended barrels are divided into 64 modules, each spanning $2\pi/64$ azimuthal angle. In the radial direction, the TileCal extends from an inner radius of $2280mm$ to an outer radius of $4230mm$. Each of the TileCal modules is composed of a grid of alternating layers of steel plates (absorber) and scintillator tiles (active material) with period of 18 mm (Fig. 1(a)). Tiles are oriented perpendicular to the colliding beams and are radially staggered in depth. The Tile calorimeter contains 11 different sizes of trapezoidal shaped tiles, ranging from about $200mm$ to $350mm$ in length and $97mm$ to $187mm$ in radial width. All tiles are $3mm$ thick. Fig. 1(b) and Table 1 give details on the tile characteristics. Each tile has two holes of $9mm$ in diameter always placed $13.5mm$ away from the tile extremity (Fig. 1(b)). Typically, the tile inner radius hole is used for metal fixing rods and the tile outer radius hole is used for the ^{137}Cs calibration tubes. In tile row 7 of EB modules both holes serve for $Cs^{137}\gamma$-source passage purposes. The scintillating tiles are read out via wavelength shifting (WLS) fibers on both sides of the tile into two separate PMTs. In LB 8 WLS fibers of different lengths are used per period per side to achieve the 3 longitudinal samplings, while in the EB 6 WLS fibers of different lengths are used, as seen in Table 1. TileCal is segmented longitudinally into three layers, which are about 1.4 (sampling A), 4.0 (sampling BC) and 1.8 (sampling D) interaction lengths thick at η=0 for Long Barrel modules. In the Extended Barrel, the second depth layer is thinner, whereas the third depth layer is thicker compared to LB modules as shown in Fig. 2. The read out cells are formed by grouping the WLS fibers into different PMTs. Cells are organized in pseudo-projective towers oriented towards the interaction point. The cell division of the 3 samplings of the Tile Calorimeter is shown in Fig. 2. The resulting cell granularity is: $\Delta\eta \times \Delta\phi = 0.1 \times 0.1$ (0.2×0.1 in the last longitudinal layer). A schematic drawing is given in Fig. 2. The details of the TileCal design, general features and expected performance can be found in [2] . More details on the scintillating tiles used in Tile calorimeter can be found in [3] and [4]

Table 1: Tile Dimensions and Cell Structure. The labeling of the dimensions corresponds to the drawing of the tile shown in Fig. 1(b)

Tile Size	A mm	B mm	H mm	E mm	Sampling		Fiber	
					LB	EB	LB	EB
1	231.0	221.3	97	70	A	A	1	1
2	240.8	231.3	97	70	A	A	2	2
3	250.6	241.0	97	70	A	A	1	1
4	262.0	249.5	127	100	B	B	3	3
5	274.8	262.3	127	100	B	B	4	4
6	287.5	275.0	127	100	B	B	3	3
7	302.3	287.8	147	120	C	B	5	4
8	317.0	302.6	147	120	C	D	6	5
9	331.7	317.3	147	120	C	D	5	6
10	350.4	332.0	187	160	D	D	7	5
11	369.0	350.7	187	160	D	D	8	6

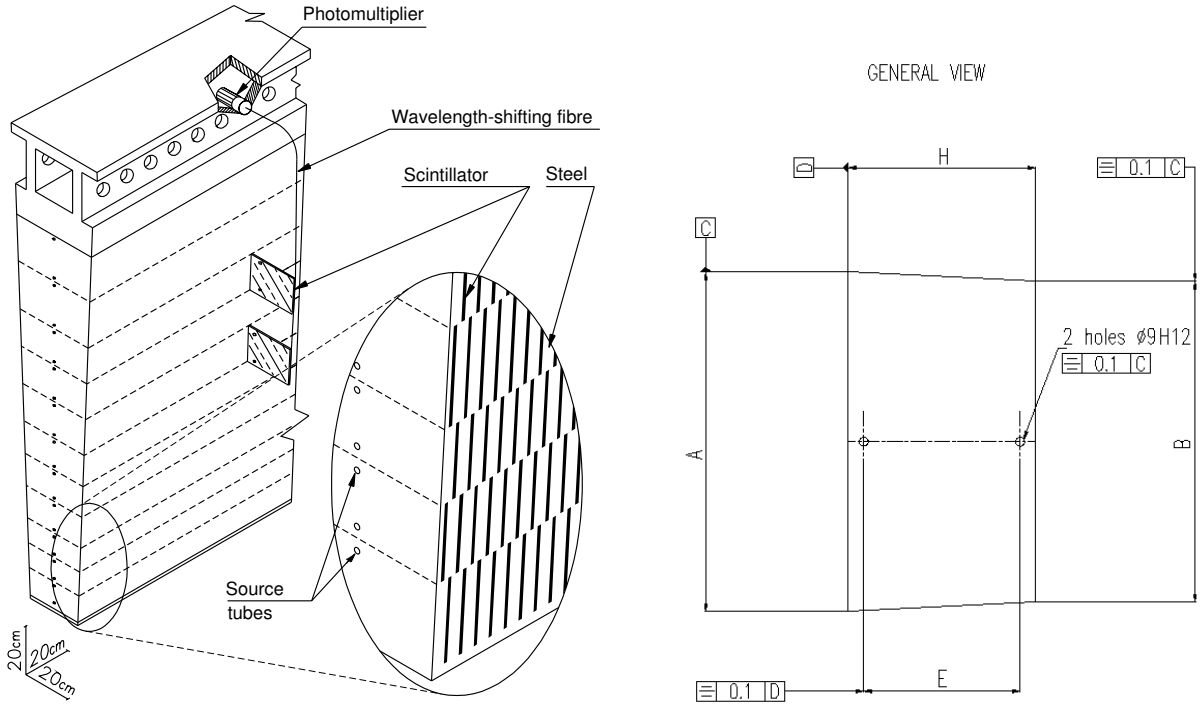

(a) Calorimeter Structure (b) Scintillating Tile

Figure 1: A blowup of the calorimeter structure (a) and drawing of a scintillating tile with the tile outer and inner radius holes for the passage of the Cs^{137} source (b).

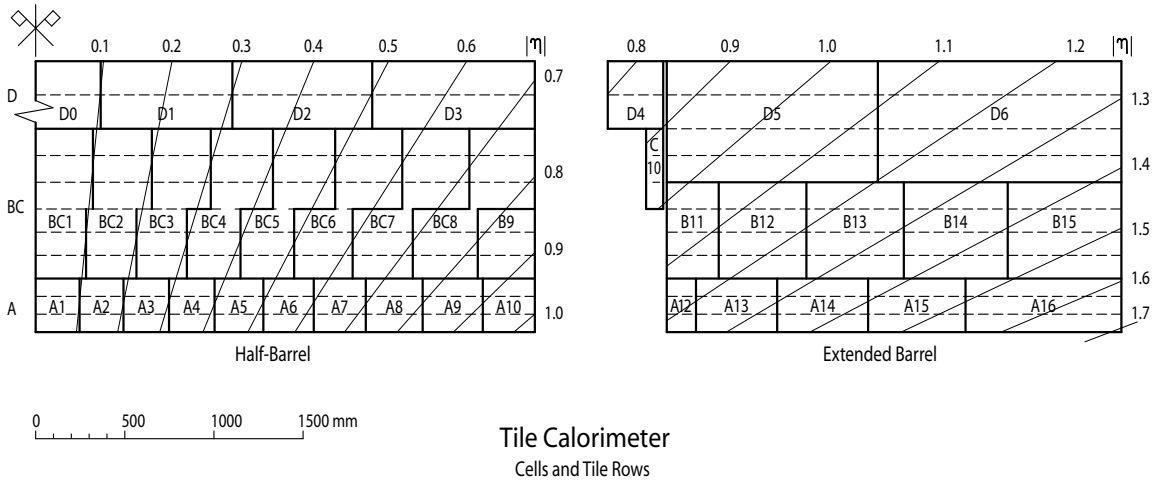

Figure 2: Layout of cells (solid lines) and tilerows (dashed lines) in the Barrel and Extended Barrel sections. The lines defining different η regions are also shown.

2 Tile Light Collection Uniformity Studies

Non-uniformity of tile response can degrade the performance of the calorimeter. Due to the size of hadron showers and the sharing of energy between the electromagnetic and the hadronic calorimeter, this effect is not as severe in the Tile Calorimeter as it is in electromagnetic calorimeters. Past studies have shown that if a random non-uniformity in the read out of the cells exists at the level of 10 % (RMS), we can expect that the constant term in the overall TileCal fractional energy resolution formula will increase by about 1 % [2]. Non-uniformity contributions arise from: non-uniformity inside a tile, tile-to-tile fluctuations, tile-to-fiber coupling, fiber-to-fiber fluctuations, variations of the response across the PMT photocathode and fluctuations inside a cell due to the fact that more than one tile is read by the same fiber. To achieve an overall response non-uniformity of $\leq 10\%$ RMS and maintain a jet energy scale precision below $1 \sim 2\%$, we kept the non-uniformities inside a tile, tile-to-tile and fiber-to-fiber fluctuations below 5% [5]. The tile-related uniformity was achieved by using black ink mask near the sides of the tiles in proximity to the fibers and by sorting the tile batches into similar light yield properties, improving the uniformity in the ϕ direction [3], [4].

In past studies of the light collection properties of scintillating tiles, we did not account for the non-uniformity of the tile surface along the radial depth direction of the ATLAS detector. The main goal of this note is to compare the light collection of the tile central region with a radius of 2.5cm (where electrons and muons incident on the calorimeter at $\theta = 90^\circ$ and 20° are used for the absolute electromagnetic calibration scale), with the light collection area around the tile outer radius hole (where the ^{137}Cs calibration source passes) and with light collection from the entire tile surface (illuminated by the hadronic shower). Section 2.1 presents the results of the tile surface uniformity studies with ^{90}Sr β-source. This note also discusses the effect of read-out fiber configuration on tile light collection and introduces the *Tile Optical Model* that describes the light collection mechanism in the trapezoidal tiles. Section 2.2 focuses on the studies with ^{137}Cs γ-sourceon individual tiles, and in Section 2.3 we describe the results of ^{137}Cs calibration scans of TileCal modules at the Test Beam and in the ATLAS pit. Section 3 presents our conclusions.

2.1 Individual Tile Measurements with ^{90}Sr β-source

2.1.1 Setup and Experimental Results

A collimated ^{90}Sr β-source with $\sim 30MBq$ intensity and electron beam size of less than 3mm (determined by the plastic collimator) was used for the tile surface uniformity studies by moving the source over the tile surface in a predefined grid as shown in Fig. 3. A dummy non-aluminized fiber was attached to the other side of the tile to provide realistic conditions of light reflection between the tile and the fiber. The measurements were done with masked tiles using a single readout fiber (of fixed length of 1 m) in the 'Standard' configuration, i.e. with the PMT close to the tile outer radius edge as in the Tile Calorimeter. The measurements with the ^{90}Sr β-source were performed with a voltmeter connected to the PMT, on the application of the source on the tile surface under high voltage. The accuracy of the measured response at a point was estimated from the dispersion of repeated measurements at all points of tile size 1 and tile size 11 and is assumed to be 4 %.

In the following the y-axis is along the TileCal radius, i.e. parallel to the line joining the holes with y=0 located at the outer radius. The x-axis is parallel to the sides of the tile.

To obtain a picture of the tile response to the ^{90}Sr source in the 'double fiber' readout configuration with additional equidistant points, we constructed a two-dimensional grid of equally

weighted points using the following procedure:

- The measured points in one half of the tile (obtained with a step size of 0.5 cm or 1 cm in the central X-strip of ± 2 cm, and with 1 cm or 2 cm step size elsewhere) were mirror reflected with respect to the plane perpendicular to the tile surface and passing through tile holes (the $X = 0$ axis) and the results were summed over. These points were considered as the measured response values at respective (X, Y) coordinates
- A grid of a fixed step size (using 1cm step) was placed over the measured points along lines parallel to X axis, by interpolating and extrapolating the measured points with a 3^{rd} degree polynomial fit. When all the X-lines were filled with these fitted points, the same procedure was applied to lines parallel to the Y axis with the same step size of 1 cm
- The grid step size was decreased to 0.25 cm and repeated once more along the X-direction and then along the Y-direction
- When the new fitted points appeared to overlap with the previously fitted points, the average number was stored.
- A 2-dimensional grid of measured and fitted points covering the entire tile surface with 0.25 cm step size was thereby obtained.

The resulting response to the ^{90}Sr β-source over the whole tile surface is shown in Fig. 4 for individual masked tiles of sizes 1 and 11 in arbitrary units. The measured points (green crosses) and the meshed fitted points is shown in the 3D response map of Fig. 4(a). The blue colored mesh represents regions with response less than the average of the tile surface, whereas the red colored mesh represents the regions with higher than the average response.

From Fig. 4(a) and 4(b) we observe a hump in the central region along the tile hole direction with response higher than the average, as well as a decrease in response in the direction from the outer to the inner radius. The slight increase of light in the central strip between the holes is due to the reflection of scintillation light from the surfaces of the holes. In the direction perpendicular to the holes a $\sim$5 % increase of light near the tile sides coupled to the fibers is observed, even in tiles masked with black ink. The increase would have been much higher (>20 %) if the tiles had not been masked [3], [4]. The RMS of the measurements in the mesh over the whole tile surface is $\sim$5 % for all tile sizes, which is well within the uniformity specifications of TileCal.

Fig. 5 shows the average response along the X (ϕ) coordinate for the case of taking the average of all the Y radial scans (red circles) and the case of taking the average of only central Y Scan values on a strip of $\pm 2.5cm$ around Y=0 (green triangles) for tile size 11. As expected, one observes the typical W-shape profile for the case of double-sided tile signal read out.

Fig. 6 shows the average tile response to the ^{90}Sr β-source along the Y radial coordinate after averaging all the X scans for tile size 1 and 11. $Y = 0$ corresponds to the outer radius extremity of the tiles. For tile size 1, $Y = 97$ mm is the inner radius extremity while for tile size 11, it is $Y = 187$ mm as shown in Table 1. The tile response to the ^{90}Sr source decreases when moving from the tile outer to inner radius holes (Y scan). This decrease is due to the trapezoidal shape of the tiles. The scintillation light is more efficiently collected at the outer radius. A detailed explanation of this effect is discussed in sections 2.1.2. and 2.1.3.

The radial decrease in scintillation light response is confirmed for all tile sizes. Fig. 7 shows the relative tile response to ^{90}Sr β-source parallel to the tile hole direction upon averaging over the central X-region of $\pm 2cm$ for all available measurements of tiles sizes 1 to 11. A clear negative slope is observed of the order of $\sim$ 1% to 2% per cm for all tile sizes. Our estimate on

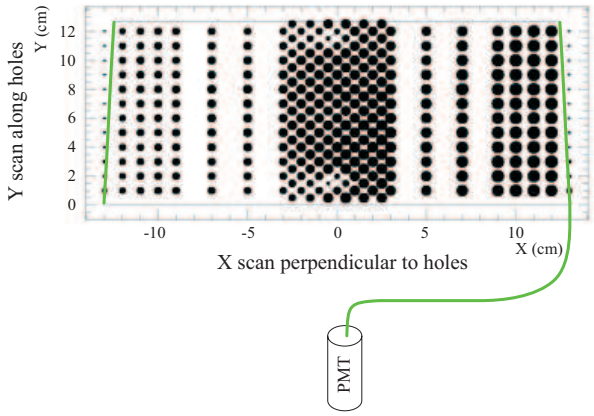

Figure 3: Schematic view on the tile with predefined grid of points for ^{90}Sr measurements in the 'Standard' configuration with single fiber readout

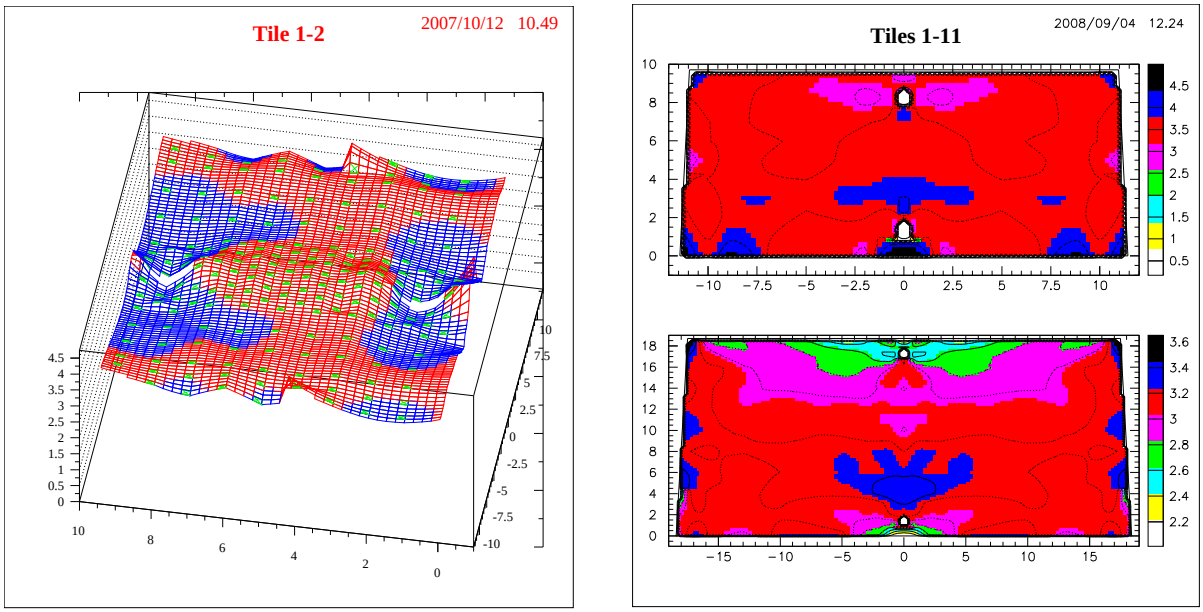

(a) 3D Scan Map

(b) 2D Scan Map

Figure 4: (a) Reconstructed 3D response of a tile to the ^{90}Sr β-source (mesh) based on individual measurements (green dots). (b) The 2D response map to ^{90}Sr of a tile size 1 (top) and a tile size 11 (bottom). The Y-axis is the one parallel to the holes and Y=0 is the outer radius edge.

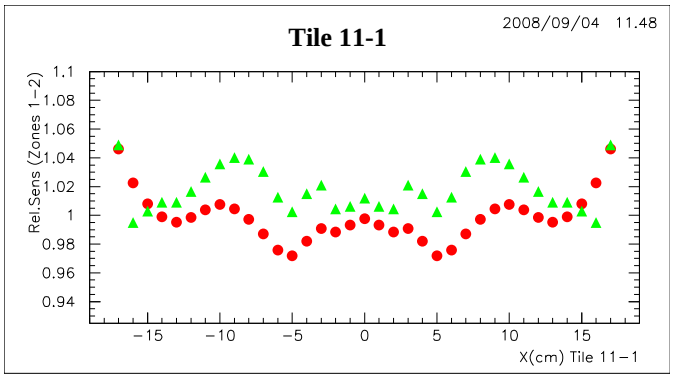

Figure 5: Tile response to ^{90}Sr-source along the $X(\phi)$ direction (perpendicular to the line joining the holes) for all Y scans (circles); Averaging only the radial scans in the central region of 2.5 cm between the holes (triangles).

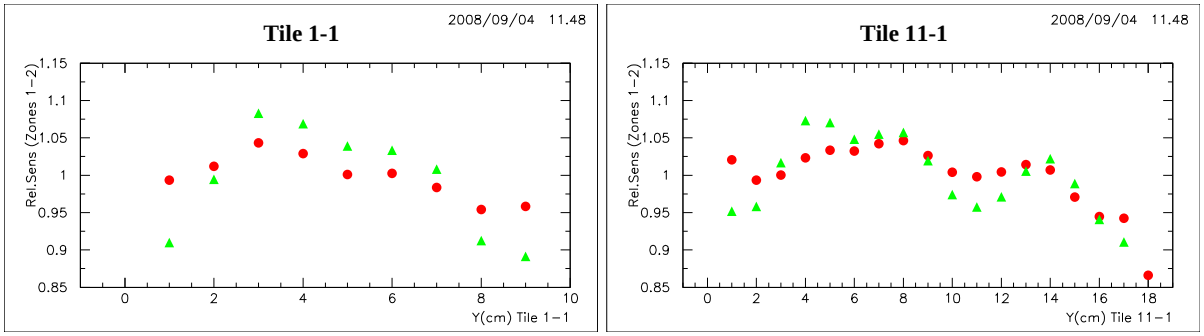

(a) Tile Size 1 (b) Tile Size 11

Figure 6: Tile response to ^{90}Sr-source along the Y radial direction (parallel to the line joining the holes) for all the X values (circles); Averaging only central Y scans in a region of 2 cm (triangles).

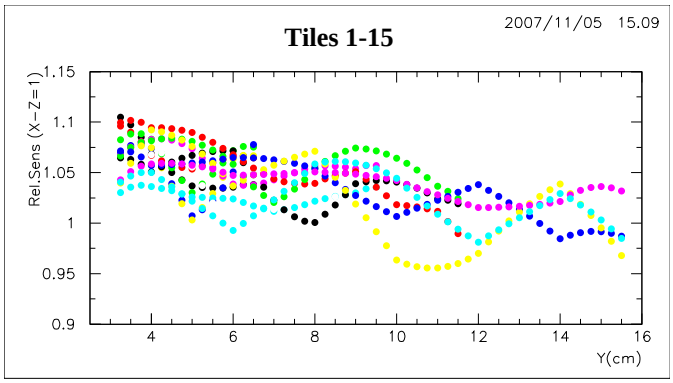

Figure 7: Relative tile response to ^{90}Sr-source along the Y radial direction. Y=0 is always the outer radius edge for all tile 11 sizes.

the statistical uncertainty of this estimate is $\sim 2\%$. The systematic uncertainty is represented by the width of the band of all 11 measurements, which on average is $\sim 7\%$. Hence the upper limit for the uncertainty can be estimated as $3 \times 2\% + 7\% = 13\%$.

A more precise quantitative estimate of this effect is achieved using measurements carried out with the ^{137}Cs γ-source going through the entire calorimeter module and sequentially exciting the areas around the inner and outer radius holes of hundreds of scintillating tiles of size 7 and several individual tiles of all 11 sizes. This is described later in sections 2.2 and 2.3.

This effect of the scintillation light collection reduction in the trapezoidal tiles when moving from the tile outer to inner radius holes gives an indication of the reason for the observed undercalibration of the middle and rear longitudinal depth cells after the calibration of TileCal with the Cesium γ-source (passing always in the outer radius holes) [6]. We set the absolute electromagnetic scale in TileCal with electrons and muons impinging the center of the tiles at $\theta = 90^\circ$ and 20° and exciting the central region of the tiles (radius of 2.5 cm), whereas TileCal cells are intercalibrated with the ^{137}Cs γ-source using the response in the area around the outer radius hole. Thus, the discrepancy between the response to electrons or muons and ^{137}Cs γ-source grows larger for larger tiles. The radial distance between these 2 regions, hence the magnitude of undercalibration, increases with the tile size (H/2 dimension) as is shown in Table 1.

The remaining question is whether or not the light response from the center of the tile is an accurate representation of its surface and how this response depends on the tile size. Fig. 8 shows the ratio of ^{90}Sr response in the central region of radius $\sim$ 2.5 cm to the response averaged over the total tile area as a function of the tile row number. This ratio is tile size independent. Fig. 8 shows this measurement for 2 sets of 15 tiles, 1 tile of each size except for tile size 1 and 11 where 3 tiles were measured. Merging the 2 tile samples (30 tiles) we obtain a mean of the ratio in the central region (radius=2.5cm) over the total tile surface of 1.03 with $RMS = 1.4\%$ as shown in Fig. 9.

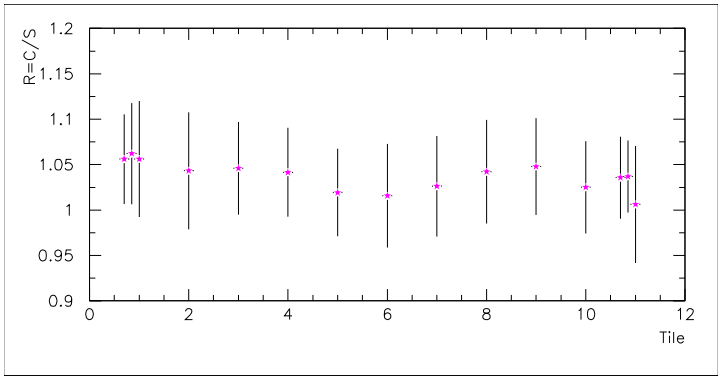

(a) March-2002 Sample.

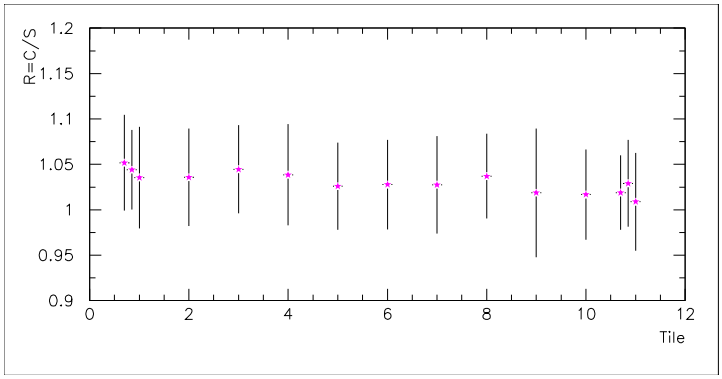

(b) April-2002 Sample

Figure 8: Ratio of the response to Sr in a circle of 2.5 cm radius located in the center of the tile over the response in the whole surface as a function of the tile raw number. Three different tiles of size 1 and 11 were measured.

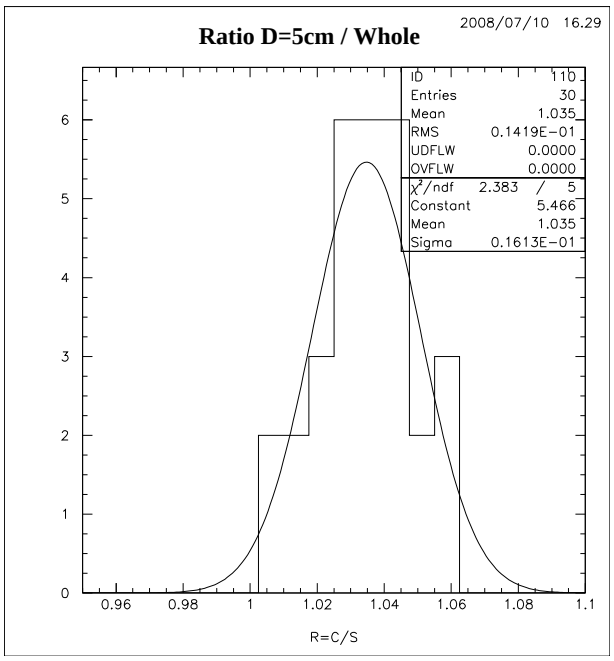

Figure 9: Ratio of the response to ^{90}Sr-source in a circle of 2.5 cm radius located in the center of the tile to the response of the whole tile surface. A sample of 30 tiles was used; 6 tiles of size 1 and 11 and 2 tiles of each size for tile sizes 2 to 10.

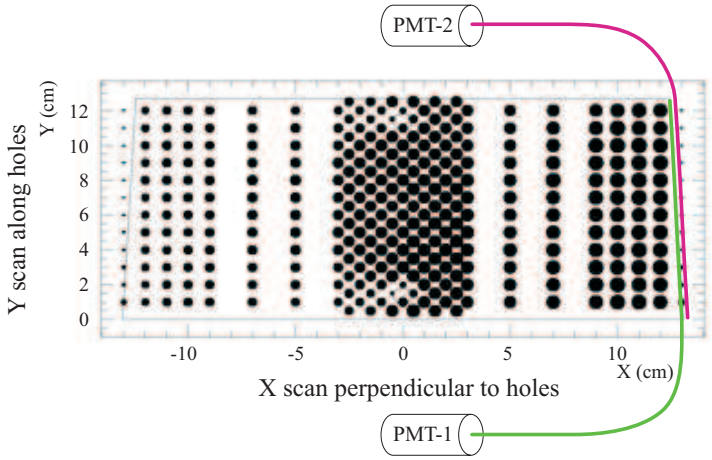

Figure 10: Scheme of fiber readout by PMT-1 as in the calorimeter with PMT-1 closer to tile outer radius. The fiber was inverted and PMT-2 placed closer to tile inner radius edge for the special test of section 2.1.2.

2.1.2 Read-out Fiber Configuration Effects on Tile Light Collection

In order to address the possible impact of the read out fiber attenuation length on light collection reduction as a function of tile radius the response of tile size 11 to the ^{90}Sr-source was measured in the Standard configuration of TileCal modules, i.e. the PMT closer to the tile outer radius edge (green fiber and PMT-1 on Fig. 10). The same measurements were also conducted in the 'Inverted' configuration, i.e. PMT closer to the tile inner radius edge (PMT-2 and pink fiber on Fig. 10). The same fiber of 97 cm length was used for both fiber configurations. Scintillating light was collected at one tile side via the WLS fiber connected to the PMT, while the other tile side was coupled to a dummy fiber. Fig. 11 shows the ratio of tile mean response in the Standard and the Inverted configurations for 7 radial scans inside the X range from +3 to +9 cm from the tile center (Fig. 10). One can see from Fig. 11 that the ratio distribution is consistent with a flat response. This is clear evidence that this effect is not correlated to the light attenuation in the WLS fibers and has to do with the tile geometry, i.e. the tile trapezoidal shape only.

2.1.3 The Tile Optical Model

In order to address the issue of tile light collection reduction from the outer to the inner radius holes described in the previous section, we developed the *Tile Optical Model*, based on simple statements of geometrical optics and Liouville's theorem. We assume here that scintillation light collection is due only to only the direct light incident on the read out WLS fiber side and single reflections from the tile sides to the WLS fiber. We further assume total internal reflection from the tile edges. More specifically, this means that the scintillation light at source S_R will be collected by the WLS read out fiber (see Fig. 12):

- Due to direct incidence on the fiber, associated with solid angle Θ_0
- Due to light reflection from the outer radius edge, an extra acceptance in solid angle Θ_1, which corresponds to an imaginary source S_I^1 at the mirror image location of S_R with respect to the tile outer radius edge.
- Similarly, an additional acceptance due to reflection from the tile inner radius edge in solid

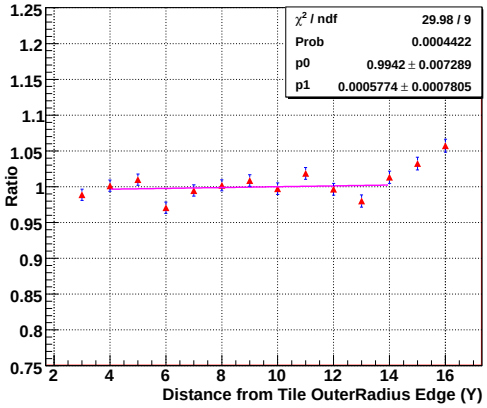

Figure 11: Ratio of average responses of the 3 cm < X < 9 cm strip of the tile to the ^{90}Sr-source along the radial direction between the normal and inverted fiber readout. A tile of size 11 is used.

angle Θ_2, corresponds to an imaginary source S_I^2 at the S_R mirror image position with respect to the tile inner radius edge.

Also note that the light collection intensity depends on the length (L) of the propagation of the light in the tile material due to light attenuation (L_{Att}) according to the $I = I_0 \exp^{-L/L_{Att}}$ rule. This means that the weights of contributions into the tile light collection are different in each of the solid angles described above. We assume further that the weight of the contribution from the tile inner (outer) radius edge reflection is negligible (i.e. its weight is zero) for the source in proximity to the outer (inner) radius tile edge, respectively.

As is well-known, Liouville's theorem states that the light flux per unit area and solid angle is constant. This means that the larger the solid angle (in which the read out fiber is seen from the source position) the greater the light flux, hence greater light collection from the source. Consider two sources S^1 and S^2 the same distance away from the tile outer and inner radius edges respectively. Both are the same distance away from the axis passing through the tile holes (see Fig. 13). Fig. 13 clearly shows that due to the tile trapezoidal shape the solid angle at S^1 is greater than the one at S^2 resulting in the light collection reduction effect from outer to inner radius described in section 2.1.1.

Based on the Tile Optical Model, one can predict that black painting the tile outer radius edge (i.e. suppressing the reflection from that edge) will result in a deterioration of tile light collection, and this degradation will be greater in proximity to the tile outer radius edge, hence resulting in flatter reduction curve (see comparison of solid and dashed lines of Fig. 14).

Similarly, black painting tile inner radius edge causes deterioration of tile light collection and this deterioration must be more notable for the region close to inner radius edge. Hence, the decrease curve should become steeper (compare solid and dash-dotted lines on Fig. 14).

To investigate further the issue of the light collection reduction and study the validity of the Tile Optical Model and predictions suggested by it, a set of measurements with collimated ^{90}Sr β-source was carried out. A collection of three different tiles without Tyvek wrapping nor masking was used. The settings of the experimental equipment are described in section 2.1.1.

Fig. 15(b) shows a comparison of light collection of the tile in the standard configuration (circles) versus that for the outer radius 3 mm thick edge painted black (triangles) as in Fig. 15(a). As can be seen, the characteristic negative slope is less steep. This is expected, since by sup-

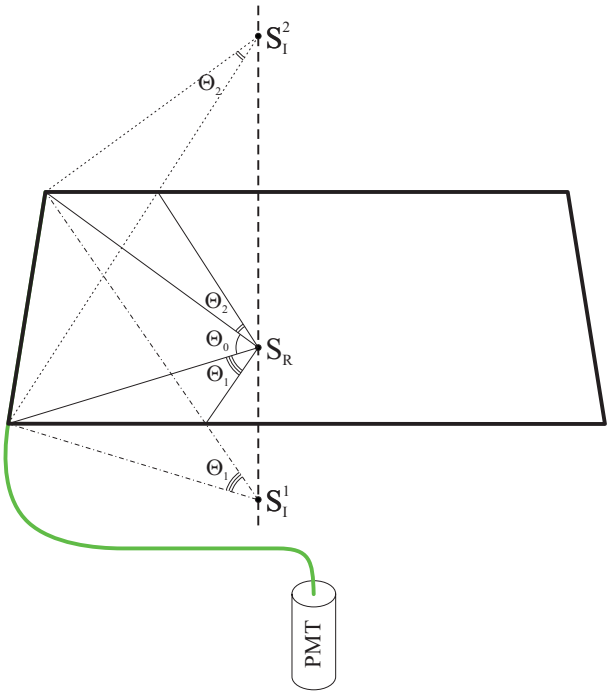

Figure 12: Schematic view of tile light collection from the source at S_R.

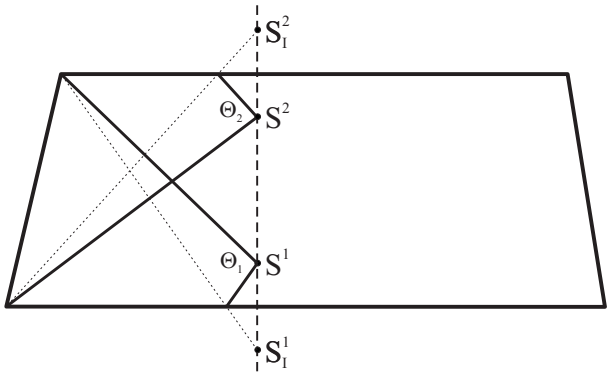

Figure 13: The comparison of light collection in the proximity to the tile inner radius (position at S^2) versus tile outer radius (position at S^1) edges.

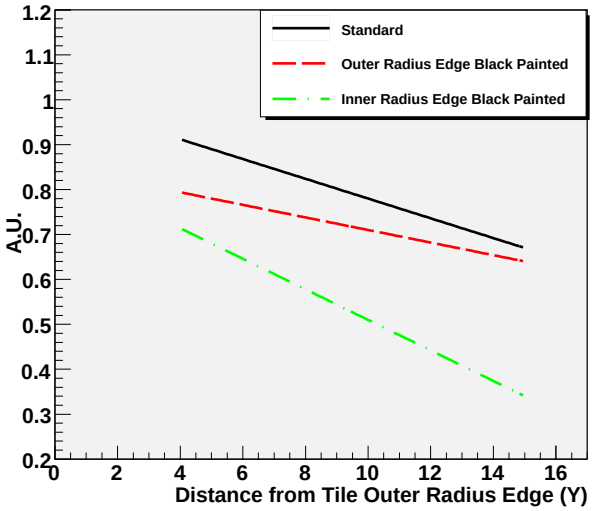

Figure 14: Prediction for the behavior of the tile light collection reduction curve for masking with black ink on the tile outer radius edge (dashed red line) versus on the inner radius edge (dash-dotted green line).

pressing the reflection from the tile outer radius edge, we essentially suppress the acceptance in the solid angle Θ_1 (see Fig. 12), the contribution of which is apparently greater when the β-source is closer to the outer tile radius edge. We also obtain good agreement between the Tile Optical Model prediction (dashed red line of Fig. 14) for the tile outer radius edge black-painted configuration with experimental data collected with ^{90}Sr β-source. One can also note from Fig. 15(b) that there is always a decreasing tail in proximity to the tile outer radius edge i.e. the region of $+3$ cm $< Y < +7$ cm. This is due to non-ideal reflection from the tile outer radius edge. Note also, that it is steeper for the black-painted case.

Fig. 16(b) shows the comparison of the tile light collection in the standard versus the tile inner radius edge black-painted configurations. One can now see that the negative slope is steeper. This can be explained by the suppression of the reflection from the tile inner radius edge, the contribution of which is more significant in proximity to the tile inner radius edge. Again, we obtain good agreement between the Tile Optical Model prediction (dash-dotted line of Fig. 14) for the tile inner radius edge black-painted configuration and experimental data collected with the ^{90}Sr β-source.

Fig. 17(b) shows the comparison of tile light collection from standard versus the side opposite to single fiber readout black-painted configurations. One can see that the reduction in slope does not change noticably. This explicitly justifies our approximation in which we neglect light collection due to double, triple etc. reflections.

Lastly, note that there is a discrepancy[4)] in light collection from three different tiles probed in the Standard configuration, which is due to tile-to-tile, tile-to-fiber optical fluctuations (compare red data curve and the red boxes of Fig. 15(b), Fig. 16(b), Fig. 17(b)). We estimate the uncertainty on the light collection reduction measurement as the ratio of the uncertainty of the 'p1' parameter (see red boxes of Fig. 15(b), Fig. 16(b), Fig. 17(b)) to its value. The numeric estimate is $30\% - 40\%$.

[4)] 1.5 % to 2.2 % per cm decrease from outer to inner radius edges from 3 different tiles.

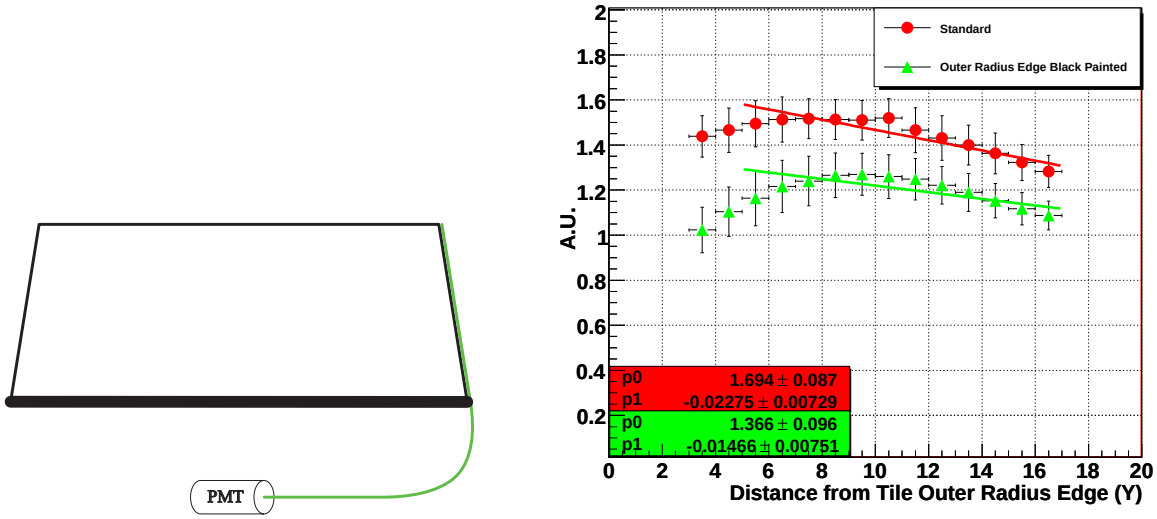

(a) Tile outer radius edge black painted configuration

(b) Tile light collection reduction curves

Figure 15: Schematic view of tile outer radius black painted configuration (a) and average response to ^{90}Sr β-source along Y radial scans in a region of $+3 < X < +9$ cm. (Circles) for tile size 11 without Tyvek in 'Standard' configuration, (triangles) after painting tile outer radius $3mm$ thick edge to suppress light reflection from that edge.

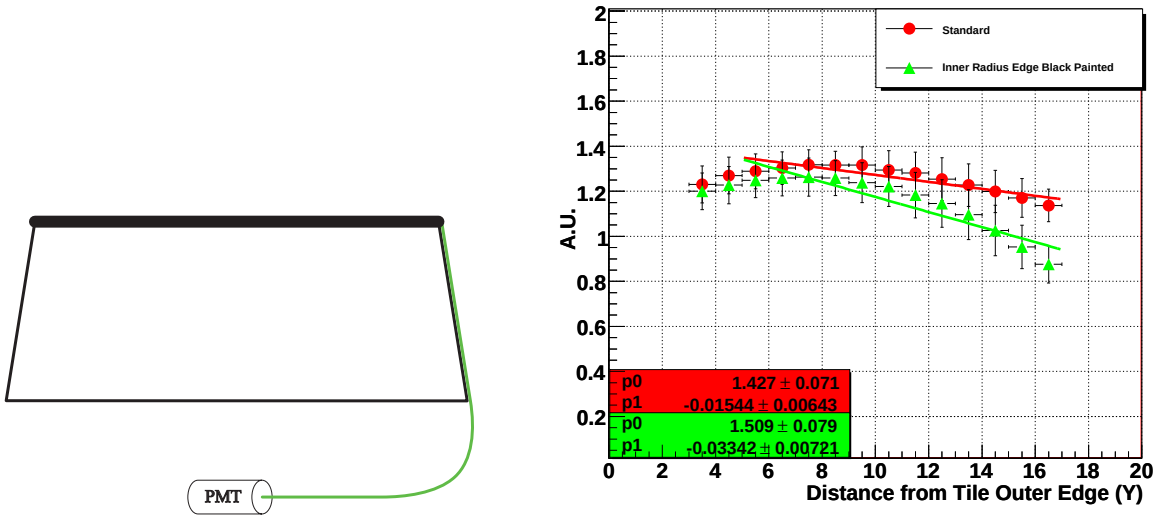

(a) Tile inner radius edge black painted configuration

(b) Tile light collection reduction curves

Figure 16: Schematic view of tile inner radius black painted configuration (a) and average response to ^{90}Sr β-source along Y radial scans in a region of $+3 < X < +9$ cm. (Circles) for tile size 11 without Tyvek in 'Standard' configuration, (triangles) after painting tile inner radius $3mm$ thick edge to suppress light reflection from that edge (b).

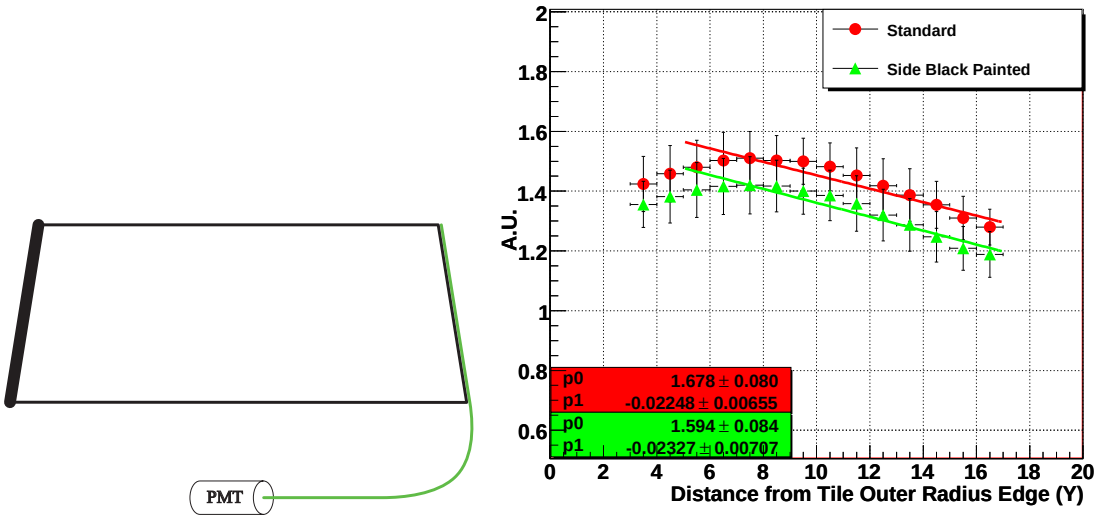

(a) Tile side (opposite to fiber read-out) black painted configuration

(b) Tile light collection reduction curves

Figure 17: Schematic view of tile side (opposite to fiber read-out) black painted configuration (a) and average response to ^{90}Sr β-source along Y radial scans in a region of $+3 < X < +9$ cm. (Circles) for tile size 11 without Tyvek in 'Standard' configuration, (triangles) after painting tile side (opposite to fiber read-out) black (b).

2.2 Measurements of Individual Tiles with ^{137}Cs γ-source

The same individual tiles that were measured with the $^{90}Sr\beta$-source (section 2.1.1), were measured in a special test bench setup at CERN in the barrel module instrumentation workshop using the ^{137}Cs γ-source calibration system [7]. Fig. 18 shows the picture of the setup.

Each of the tiles was positioned on the Cs γ-source tube in between two steel plates $10mm$ thick. The scintillation light was collected from both tile sides connected to a PMT in the drawer. The response of the individual tile was defined as the amplitude of the fit of the tile response curve. Fig. 19 depicts a typical fit for an individual tile response curve. For the individual tile measurements the response to the ^{137}Cs γ-source was measured for the source passing through the outer and the inner tile radius holes.

Fig. 20(a) shows that the tile response to ^{137}Cs γ-source (circles) passing through the outer radius hole for the case of larger tile sizes is overestimated compared to the tile response from the whole tile surface as obtained using the ^{90}Sr β-source (triangles). This figure should be treated as a qualitative illustration of this effect. The experimental uncertainties associated with the square points are dominated by the fact that the ^{137}Cs and ^{90}Sr measurements were done using two different setups. The tile outer radius hole was enlarged to enable the passage of the Cs γ-source and the tile/fiber coupling was changed for these two measurements. It is an independent verification of the light collection reduction effect as observed in other ^{90}Sr β-source studies (section 2.1.1). One should also note that the ratio presented in Fig. 20(a) (triangles) was also depicted in Fig. 8(b) for the same sample of 15 tiles. Our estimate on the statistical uncertainty (using the measurement for the tile size 9) is $\sim 7\%$ and the systematic uncertainty is $\sim 17\%$. Hence the upper limit of the uncertainty can be estimated to be $3 \times 7\% + 17\% = 38\%$.

More precise evidence of this effect is depicted in Fig. 20(b), showing the ratio of the response

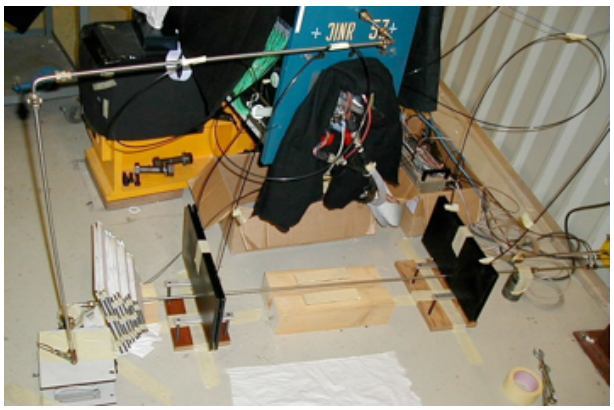

Figure 18: Setup for measuring individual tiles response with ^{137}Cs γ-source at the instrumentation lab

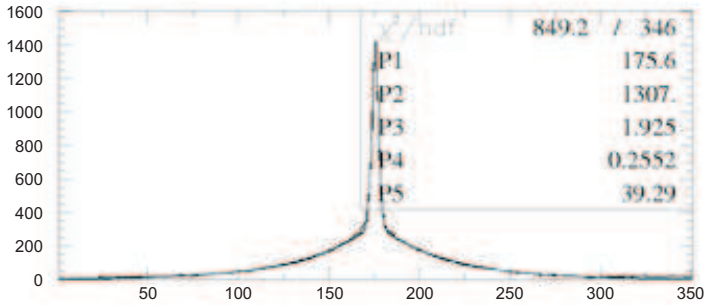

Figure 19: Typical fitted response of one tile to ^{137}Cs γ-source in the setup of Fig. 18

of the probed tile to ^{137}Cs γ-source passing through the inner radius hole to the response at the outer radius one. One clearly sees the light collection reduction effect dependence on tile size. From these measurements the estimate of light collection reduction from the tile outer radius hole to the inner radius hole is on average $\sim 0.8\%$ per cm. For example, for tile row 7 (where the distance between holes is 12 cm) the ratio $R(O/I) = 1/0.91 = 1.1$ or 0.83% per cm. The uncertainty on this measurement can be estimated as the repeatability of the measurement, which for tile size 9 is 15%. This value is compatible with the value obtained with the ^{90}Sr measurements described in section 2.1.1. In the next section we will compare this value with the one computed from Cesium source data at the Test Beam over a sample of $\sim 10\%$ of EB modules and data collected at Cesium source scans of the majority of the EBC modules during cesium source calibration runs in the pit.

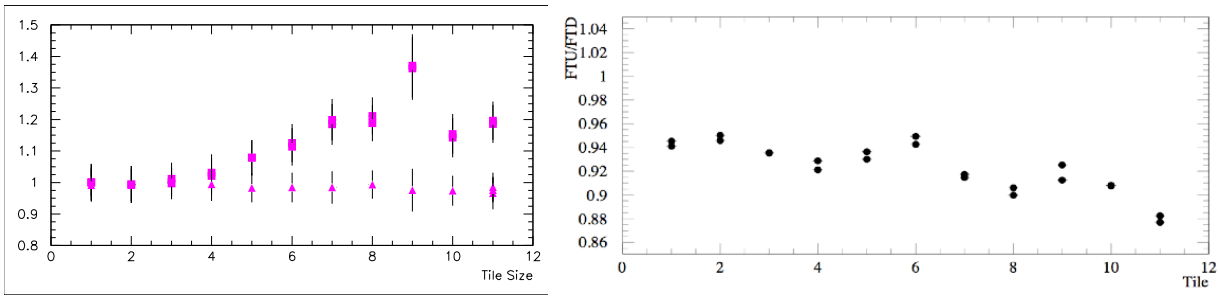

(a) (b)

Figure 20: (a) The ratio of the response to ^{90}Sr of the tile central region with 5 cm diameter (outer hole region) to tile overall surface (triangles) and the ratio of response to ^{137}Cs to the response to ^{90}Sr of the tile overall surface (circles) vs tile size (1 to 11), both sets normalized to the corresponding ratio at tile size 1. (b) The ratio of response to ^{137}Cs γ-source at the source passage from the inner radius over the one at the passage through the outer radius hole, tile sizes 1 to 11.

2.3 ^{137}Cs γ-source in TileCal Modules

2.3.1 The Setup at TB and in the ATLAS Pit

As described in section 1, each scintillating tile has two 9.0 mm diameter holes positioned always at the same distance ($13.5mm$) from the inner and the outer radius edges where the ^{137}Cs calibration source will pass through. A schematic view of the barrel module tube installation is shown in Fig. 21(a). The capsule containing the radioactive ~ 10 mCi ^{137}Cs γ-source is carried along by a liquid flowing inside the calibration tubes passing through all cells of the calorimeter, hence measuring the response and monitoring the optical quality of more than 463000 tiles coupled to fibers in all 192 TileCal modules [8]. Typically the Cesium source passes through the tile outer radius hole. Fig. 21(b) shows the concept of the γ-source path in a calorimeter module. The cesium tube installation has a peculiarity in the EB modules, since in those, the ^{137}Cs γ-source passes through both holes in tile row 7. This enables an independent estimate on the light collection reduction between the outer radius and the inner radius regions, similar to what was previously presented for individual tiles with ^{90}Sr and ^{137}Cs systems. The advantage of exciting many tiles of the same size at the same time allows reducing the effect of optical fluctuations that are present in individual tile measurements compared to the thousands of tiles

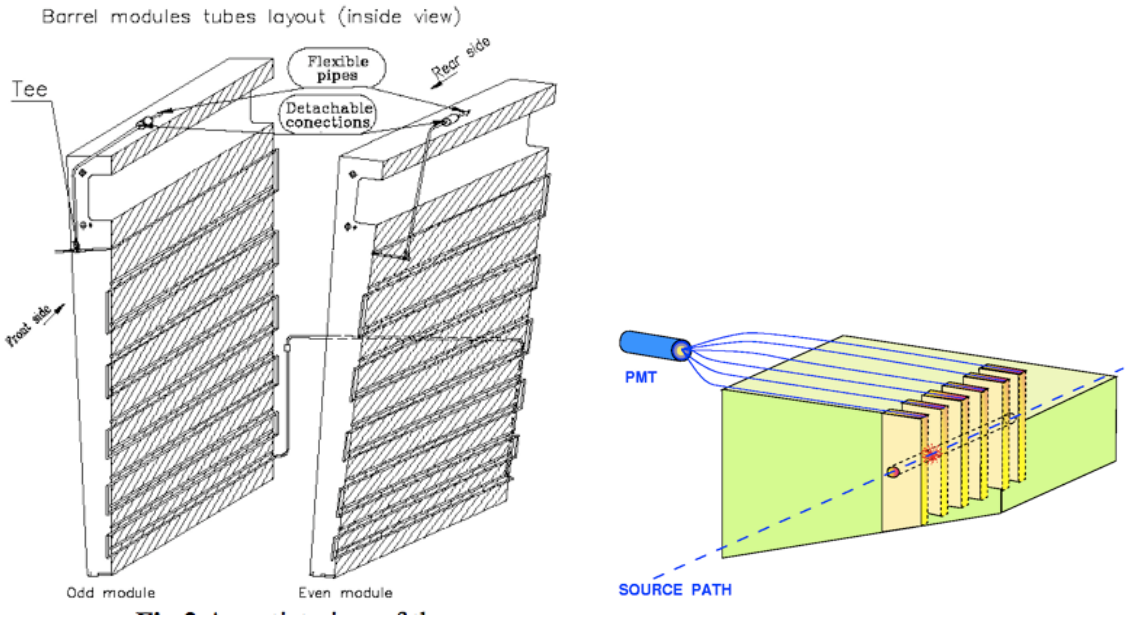

(a) (b)

Figure 21: (a) Schematics of source path in TileCal. (b) Source passing through a tile row in a cell.

excited inside the Tilecal modules. As opposed to studies of individual tile response to ^{137}Cs γ-source, when the quantitative estimate of this effect is simply the ratio of the tile responses for tile outer to inner hole cases, the studies of the γ-source scans of the entire tile module have to address carefully the issue of energy leak to the adjacent tile row. In the EB modules tile row 7 and 6 belong to BC cells while tile row 8 belongs to D cells. Hence, when computing the response of tile 7 with Cs source passing through the inner radius hole, the leakage from tile row 7 to 6 must be taken into account. The method used to unfold the effect of leakage between tile rows is addressed in Appendix A.

2.3.2 Results of ^{137}Cs Scans at Test Beam and in the ATLAS Pit

As was mentioned in section 2.2, the quantitative measure of the light collection reduction effect is the ratio of tile response to ^{137}Cs γ-source passing through the tile outer radius hole to the response at the tile inner radius hole; R(O/I). The distribution of that ratio estimated from the data collected during the calibration runs in the Test Beam in periods 2001 to 2004 is presented in Fig. 22(a). We use this data to measure the $Mean = 1.104$ and $RMS = 11\%$ for R(O/I). The Leakage to the adjacent tile row is corrected for. The ^{137}Cs leakage corrections in Tile 7 outer and inner radius holes are discussed in detail in appendix A. The length of the fibers reading out the tiles in those cells vary between $160cm$ and $190cm$ [3]. Fig. 22(b) provides evidence of η-uniformity of the measured ratio R(O/I) reinforcing the conclusions described in section 2.1.3, e.g. the WLS fiber plays no role in the reduction of the light collection along the tile radius. We remind the reader that the typical effective attenuation of these aluminized fibers is more than 3 m [5].

Similar results were acquired by the analysis of ^{137}Cs scans of the entire EBC partition of

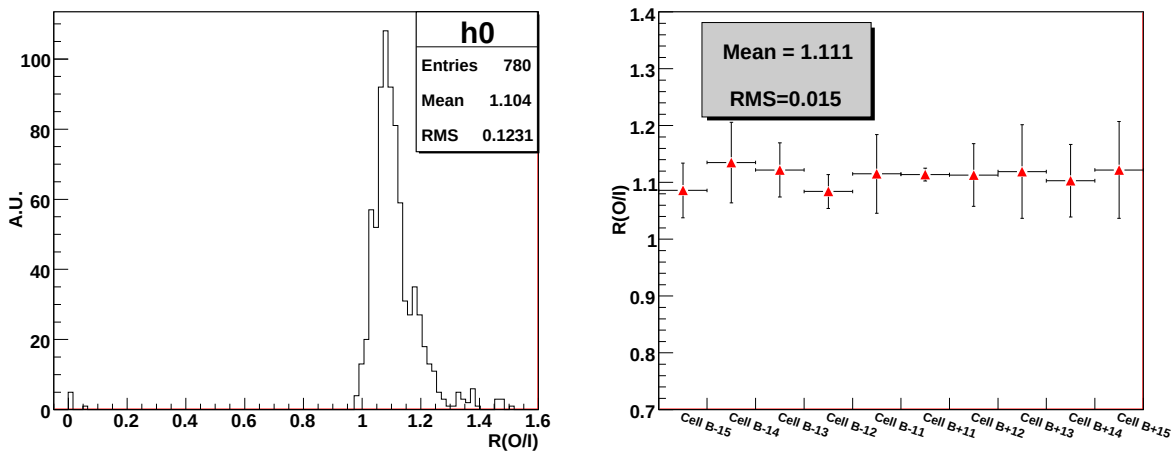

(a) (b)

Figure 22: (a) Distribution of the ratio of the tile row 7 responses to Cs at its passage through the outer radius hole over the inner radius hole. (b) The same ratio for all the B cells' tile row 7 vs the cell position. The sample represents multiple runs of the testbeam EB calibrated modules.

TileCal in the ATLAS pit. Those results are shown in Fig. 23 and confirm with high statistics[5)] that the tile response to the ^{137}Cs γ-source is $\sim 10\%$ higher in the outer radius hole than in the inner radius hole for tile size 7, compatible with the values extracted from the ^{137}Cs and ^{90}Sr results done on individual tiles (Fig. 4, Fig. 6, Fig. 20(b)). We remind the reader that the distance between the holes in tile 7 is 120 mm leading to an average reduction of the light collection between the holes of 0.87% per cm.

2.3.3 The Effect of Tile Polystyrene Type on Light Collection

Two types of polystyrene were used for the TileCal module instrumentation; BASF and PSM [4], [9]. Concerning the polystyrene types of BC and D cells in TileCal there are three families of modules; ones instrumented with BASF tiles only, another with PSM tiles and a third with mixed types. We show below that the above-mentioned effect of light collection reduction as a function of tile depth is tile polystyrene type independent. The evidence for this is shown in Fig. 24 where we present the distribution of the ratio R(O/I) of the tile response to Cs source passing through holes at the outer radius to response at the inner radius. The upper plot of Fig. 24 shows the ratio R(O/I) for modules instrumented exclusively with PSM tiles, whereas the lower plot shows the R(O/I) ratio for modules only with BASF tiles. For the measured values of the R(O/I) distribution for PSM modules is $Mean = 1.1$ with $RMS = 4.5\%$ and for BASF modules we measured $Mean = 1.107$ with $RMS = 5.4\%$. Hence, within RMS uncertainties, we report the same values for both polystyrene cases.

[5)] The statistics of Fig. 22(a) is from multiple runs on the EB modules exposed to test beam. The statistics of Fig. 23(a) is a subset of the B-cells in a single EBC run in ATLAS.

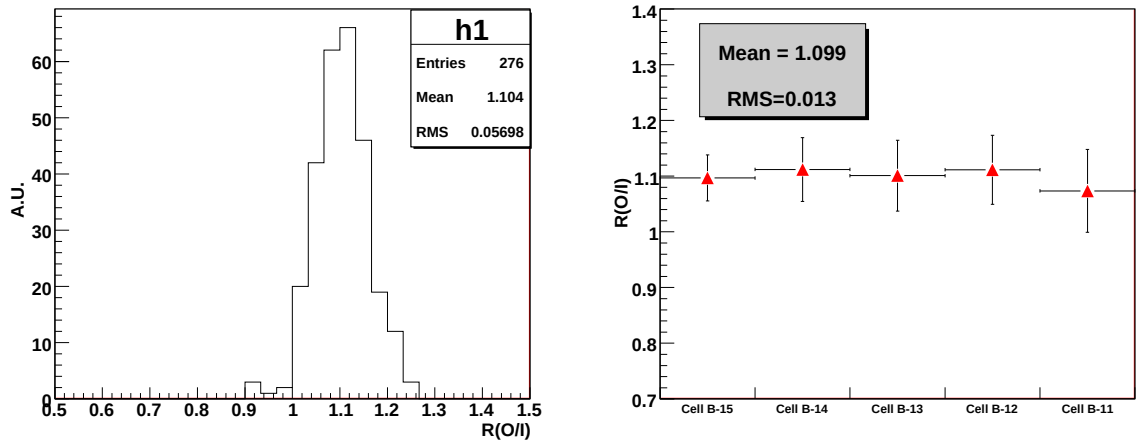

(a) (b)

Figure 23: (a) Distribution of the ratio of the tile row 7 responses to Cs at its passage through the outer radius hole to that for the inner radius hole. (b) The same ratio for all the B cells' tile row 7 vs the cell position. The sample is a fraction of the EBC modules.

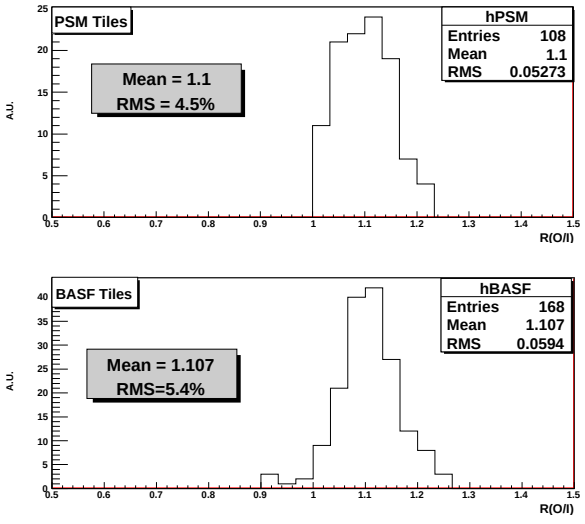

Figure 24: Distribution of the ratio of the tile size 7 responses to ^{137}Cs at its passage through the outer radius hole over the inner radius hole for modules with tiles made from PSM (top) and BASF scintillator (bottom).

3 Conclusions

The ^{137}Cs system is the main tool to equalize the response from all of the TileCal cells via setting the PMT HV in an iterative procedure. The absolute energy scale or the pC/GeV conversion scale was determined with electrons and muons impinging the calorimeter at the centre of tiles at $\theta = 20^{\circ}$ and 90° [6]. This created the necessity for us to study and take into consideration possible differences of TileCal cell response to real particles versus the ^{137}Cs γ-source, since it was reported that the ^{137}Cs weights, obtained with the amplitude method, in BC and D cells are underestimated by 2.5% and $\sim$ 8.8% respectively for the barrel and 0.9% and 5.5% for the EB [6].

In this note we presented the reason for this, which is the difference in response between particles ($e^{\pm}$, $\mu^{\pm}$) and ^{137}Cs γ-source, which grows larger for larger tile sizes. The previously observed decrease in the e/Cs and μ/Cs ratios as a function of the tile size (1 to 11) is attributed to the light collection decrease from the outer to the inner radius sides of the tiles. This decrease, as extracted by several independent ^{137}Cs and ^{90}Sr measurements is shown in Table 2.

The level of decrease that would be consistent with the undercalibration of BC and D cells mentioned above is 1.5% to 2% per cm in the radial direction of the ATLAS detector. The ideal sample to precisely extract the extra correction factors for the BC and D cells would be fine muon radial scans between the source passage holes. Unfortunately such testbeam samples are not available. Our results support the need for additional corrections to the electromagnetic scale factor in BC and D cells as reported in [6]. Our investigation showed that there is no dependence on the fiber attenuation or the type of polystyrene used in tile production. The light collection reduction effect is due to the trapezoidal shape of the tile and the fact that the tile radial depth changes with longitudinal layer.

Table 2: Summary of the light collection reduction measurements along tile radius.

Source	Sample	Reference Figure	Measurement (% per cm)	Uncert.
^{137}Cs scans in the pit and TB, outer/inner radius response ratio	Tile 7, $\sim$ 200 B-cells	22(a), 23(a)	0.9 %	11 %
^{137}Cs scans of individual tiles, outer/inner radius response ratio	All sizes, 30 tiles	20(b)	0.8 %	15%
^{90}Sr individual tile scans	Tile 11, 3 tiles	15(b), 16(b), 17(b)	1.5 % to 2.2 %	30%-40%
^{90}Sr individual tile scans	1 tile per size	7	1 % to 2 %	13%
^{137}Cs outer radius hole over ^{90}Sr(surface average) ratio	All sizes, 30 tiles	20(a)	2 % to 4 %	38%

References

[1] The ATLAS Collaboration, G. Aad et al., The ATLAS Experiment at the CERN Large Hadron Collider, (JINST 3 S08003,2008), .

[2] ATLAS Collaboration, Tile Calorimeter Technical Design Report (1996).

[3] P. Amaral et al, ATL-COM-TILECAL-2008-011 (2008).

[4] A. Abdallah et al, ATL-TILECAL-PUB-2007-010 (ATL-COM-TILECAL-2007-026) (2007).

[5] A. Gomes et al., ATL-TILECAL-2002-011 (2002).

[6] Anderson K. J., ATL-TILE-COM-2008-016 (2008).

[7] E.Starchenko et al., NIM A 494 (2002) 381-384, TILECAL-2002-003 (2002).

[8] E.Starchenko A. Zenine, http://indico.cern.ch/getFile.py/access?contribId=29 (TileCal Week Oct 2001).

[9] J. Abdallah et al, ATL-TILECAL-PUB-2008-005 ; ATL-COM-TILECAL-2007-025 (2008).

4 Appendix A

Energy Leak from Tile Row to Tile Row at ^{137}Cs γ-source Passage in TileCal Modules

The response of a cell is determined as the mean of individual tile response amplitudes over the time interval corresponding to cell limits (see Fig. 25(a))

$$I = I_{left} + I_{center} + I_{right} \tag{1}$$

A typical picture of a cell response as a function of γ-source position in the Cesium tube is depicted in Fig. 26. From top to bottom one can see the response of the A cell tile row 3 to 1. One can note that the response of tile row 3 is $\sim 25\%$ less than ones from tile rows 2 and 3. This is due to the fact that the energy leakage from tile row 3 to adjacent tile row 4 is belongs to B cells and hence is not registered by the A cell PMTs. When the ^{137}Cs γ-source passes through the tile row, the radiation energy is uniformly distributed around the source path in a cylindrical shape (see Fig. 25(b)). This causes an energy leakage from the actual tile row into the adjacent row. Therefore, to have a good quantitative estimate of the light collection reduction along the tile depth one needs to develop a model for accurate estimation of tile to tile energy leakage.

The main assumptions of the *Energy Leakage Model* are:

- The energy transfers across the boundary between any pair of tile rows is the same
- Light collection depends only on:
  - Geometry of the tile (the trapezoidal shape). Hence, we introduce light collection coefficients R_I and R_O, which describe the tile geometrical features when ^{137}Cs γ-source passes through tile inner and tile outer radius holes, respectively.
  - Depth of the tile.
  - Energy deposited in the cell.
- Light collection does not depend on
  - Tile width
  - Read out fiber length (discussed in section 2.1.3)
  - Tile material, i.e. tile sensitivity or the ability for energy-to-light conversion.

Notation

E_0 energy deposit into tiles by ^{137}Cs γ-source

ΔE energy transfer across the tile boundary

S optical sensitivity of tile material

R_I light collection geometrical coefficient at the tile inner radius edge

R_O light collection geometrical coefficient at the tile outer radius edge

I_N measured response of a cell when the ^{137}Cs γ-source passes through tube N

I_N^0 pure response of a cell (excluding the energy leakage component) when the ^{137}Cs γ-source passes through tube N

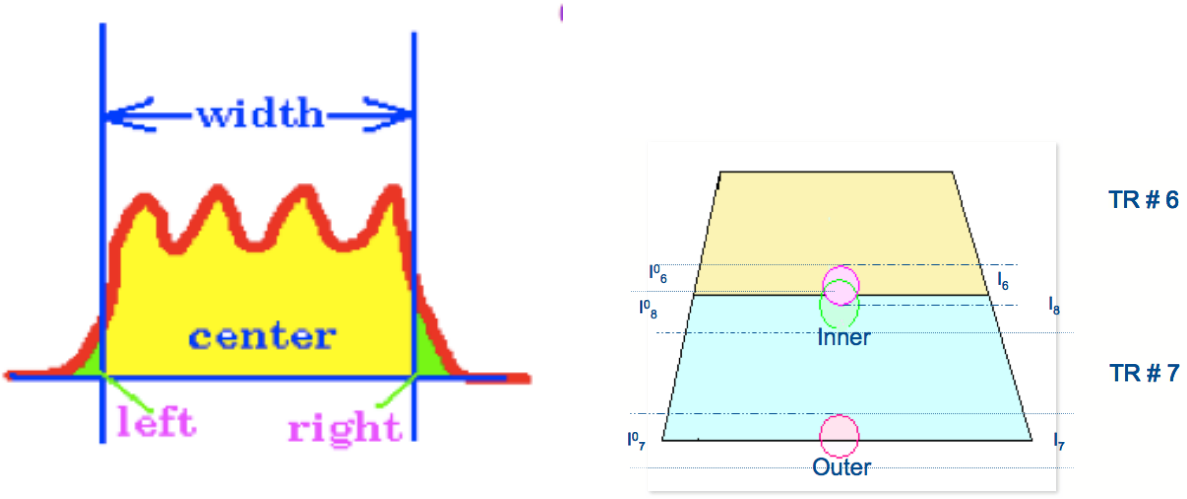

(a) (b)

Figure 25: (a) Sketch of quantitative measurment of tile light collection to ^{137}Cs γ-source. (b) Two adjacent tiles in the radial direction.

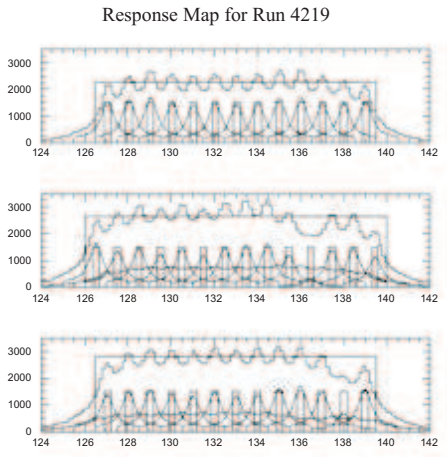

Figure 26: Typical response to ^{137}Cs γ-source vs position inside a cell with the individual tile amplitudes unfolded.

Hence, based on the assumptions described above the generic expression for cell response will be:

$$I = E \times S \times R \tag{2}$$

This enables us to write the equations of energy balance when ^{137}Cs γ-source passes through cesium tubes 6,7,8.

$$\begin{aligned} I_6^0 &= (E_0 - \Delta E) \times R_O = I_6 - \Delta \times R_I & (3)\\ I_8^0 &= (E_0 - \Delta E) \times R_I = I_8 - \Delta \times R_O & (4)\\ I_7^0 &= (E_0 - \Delta E) \times R_O = I_7 & (5) \end{aligned}$$

We define the inverse of the light collection reduction ratio along the tile depth as:

$$1/R(O/I) = I_7^0/I_8^0 = (E_0 - \Delta E) \times R_O/(E_0 - \Delta E) \times R_I \tag{6}$$

Hence,

$$R(O/I) = R_O/R_I \tag{7}$$

Upon some simple algebraic manipulations, one obtains:

$$(1/R)^2 - (I_8/I_7) \times (1/R) + (I_6 - I_7)/I_7 = 0 \tag{8}$$

The term $\alpha \equiv (I_6 - I_7)/I_7$ is the so-called leakage parameter which describes the ratio of the light collected in tile row 7 with ^{137}Cs γ-source traveling in tube 6, to the case with the ^{137}Cs γ-source traversing the module in tube 7.

The term $\beta \equiv I_8/I_7$ is the light collection reduction ratio in the no-leakage scenario. Both parameters α and β are determined by the optical and geometrical properties of tiles in row 6 and 7. Since we assumed that those properties are similar, we expect the experimentally measured values of those parameters should converge to some mean value. The distribution of the α-parameter per EB cell is presented in Fig 27(a), with measured $Mean = 0.268$ and $RMS = 0.051$.

The data was collected during the test beam period 2001/2004. The mean values are well fitted with a horizontal line demonstrating that the α-parameter values measured in various cells are statistically compatible with each other, and hence can be combined. Fig. 27(b) depicts all measured values of α-parameter with fitted offset value $p_0 = 0.263 \pm 0.013$. One can note that the mean of the latter distribution and the horizontal fit offset are in good agreement within the RMS uncertainties, suggesting validation of the Leakage model under consideration.

Another validation test is a comparison of the $R(O/I)$ value distribution for the cases of free and fixed (α= 0.268 determined from Fig. 27(b)) α-parameter values (see Fig. 28(a) and Fig. 28(b)) respectively.

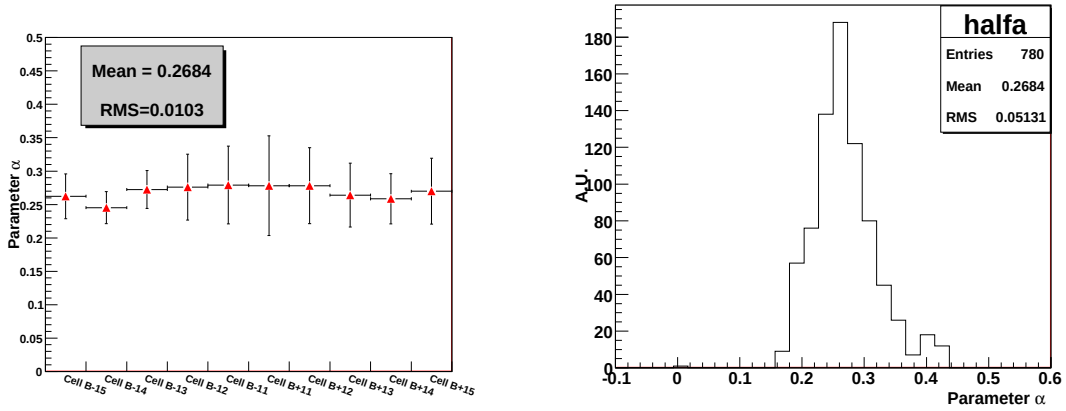

(a) (b)

Figure 27: (a) Leakage parameter between tile rows vs B cell position in the Extended Barrel. (b) Leakage parameter from the EB modules calibrated at the testbeam

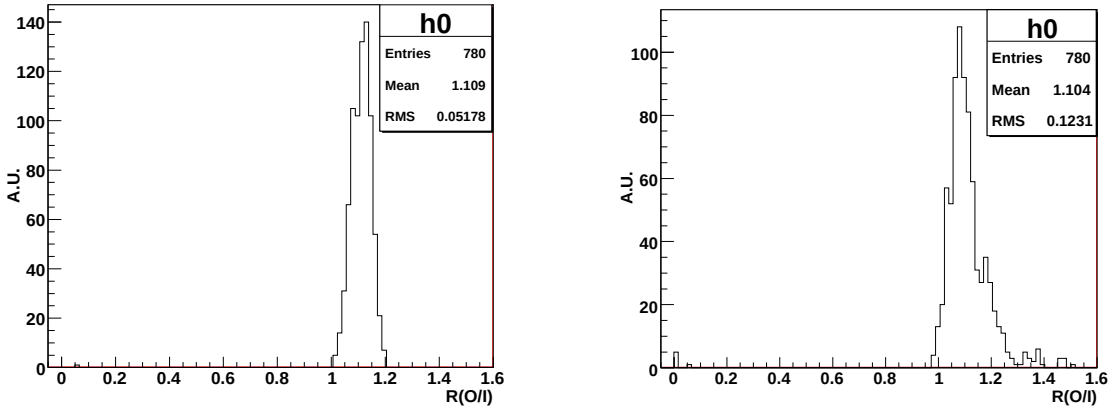

(a) (b)

Figure 28: Distribution of R(O/I) responses to ^{137}Cs γ-source with leakage parameter fixed (a) and free (b).